Towards operational use of aircraft-derived observations: a case study at London Heathrow airport

Article

Accepted Version

Mirza, A. K. ORCID: https://orcid.org/0000-0001-6350-9080, Ballard, S. P., Dance, S. L. ORCID: https://orcid.org/0000-0003-1690-3338, Rooney, G. G. and Stone, E. K. (2019) Towards operational use of aircraft-derived observations: a case study at London Heathrow airport. Meteorological Applications, 26 (4). pp. 542-555. ISSN 1469-8080 doi: 10.1002/met.1782 Available at https://centaur.reading.ac.uk/81843/

It is advisable to refer to the publisher's version if you intend to cite from the work. See Guidance on citing.

To link to this article DOI: http://dx.doi.org/10.1002/met.1782

Publisher: Royal Meteorological Society

www.reading.ac.uk/centaur

CentAUR

Central Archive at the University of Reading

Reading's research outputs online

Towards operational use of aircraft-derived observations: a case study at London Heathrow airport.

Andrew K. Mirza [*1], Susan P. Ballard[2], Sarah L. Dance[3], Gabriel G. Rooney[1], and Edmund K. Stone[1]

[1]Met Office, Exeter, United Kingdom, EX1 3PB

[2]MetOffice@Reading, Department of Meteorology, University of Reading, Reading, United Kingdom, RG6 6BB

[3]School of Mathematical, Physical and Computational Sciences, University of Reading, Reading, United Kingdom, RG6 6BB

January 25, 2019

1 Abstract

Mode-Selective Enhanced Surveillance (Mode-S EHS) aircraft reports can be collected at a low-cost, and are readily available around busy airports. The new work presented here demonstrates that observations derived from Mode-S EHS reports can be used to study the evolution of temperature inversions since the data have a high spatial and temporal frequency. This is illustrated by a case study centred around London Heathrow airport for the period 4 to 5 January 2015. Using Mode-S EHS reports from multiple aircraft and after applying quality control criteria, vertical temperature profiles are constructed by aggregating these reports at discrete intervals between the surface and 3000 m. To improve these derived temperatures, four smoothing methods using low-pass filters are evaluated. The effect of smoothing reduces the variance in the aircraft derived temperature by approximately half. After smoothing, the temperature variance between the altitudes 3000 m and 1000 m is 1 K to 2 K; and below 1000 m it is 2 K to 4 K. While the differences between the four smoothing methods are small, exponential smoothing is favoured because it uses all available Mode-S EHS reports. The resulting vertical profiles may be useful in operational meteorology for identifying elevated temperature inversions above 1000 m. However, below 1000 m they are less useful because of the reduced precision of the reported Mach number. A better source of in situ temperature observations

---
[*]Corresponding author: akmirza@mail.com

would be for aircraft to use the meteorological reporting function of their automatic dependent surveillance (ADS) system.

1   Introduction

Weather impacts on airports are an important problem for society (Ball *et al.*, 2007; Markovic *et al.*, 2008; Barnhart *et al.*, 2012). In particular, fog and low visibility conditions reduce the air-traffic flow rates at airports as aircraft separations need to be increased to maintain safe operations. The reduced flow rate increases costs in terms of the extra fuel that must be used, loss of revenue due to reduced capacity at airports, environmental impacts on local air quality and noise emissions, and climate impacts due to increased emissions of nitrogen oxides and carbon dioxide (Mahashabde *et al.*, 2011). Numerical weather prediction (NWP) forecasting fog and low visibility conditions is difficult since these require an accurate representation of orography, surface, boundary-layer fluxes and inversions in the vertical temperature profile (Stull, 2000; Jacobs *et al.*, 2008). Operational forecasting of temperature inversions depends on the availability of suitable observations (Roach *et al.*, 1976; Jacobs *et al.*, 2005; Fowler *et al.*, 2011) to locate the inversion. For example high-frequency reporting of vertical profiles of temperature and wind may provide extra information for use in NWP assimilation and nowcasting (Dance, 2004; Rennie *et al.*, 2011; Simonin *et al.*, 2014; Sun *et al.*, 2014; Ballard *et al.*, 2015; James and Benjamin, 2017). Furthermore several authors (de Haan and Stoffelen, 2012; de Haan, 2013; Strajnar *et al.*, 2015; Lange and Janjic, 2016) have demonstrated positive impacts in regional NWP models when assimilating derived observations from aircraft reports using Mode-Selective (Mode-S) Enhanced Surveillance (EHS), a system which transmits binary coded messages to an aircraft's transponder and receives binary coded replies (Boisvert and Orlando, 1993; ICAO, 2010).

Strajnar *et al.* (2015, figure 7) showed that meteorological routine air reports (MRAR) of ambient temperature, obtained from the secondary surveillance radar (SSR) using Mode-S, centred around Ljubljana airport, Slovenia, have a spatial and temporal resolution sufficient to locate a temperature inversion at around 1000 m above the surface. However, direct reports of ambient temperature using Mode-S MRAR is not routinely available since not all SSRs and not all aircraft are configured to make such reports. De Haan (2011) showed that Mode-S EHS reports of Mach number and true-airspeed, centred around Schipol airport, Netherlands, could be used to derive ambient temperature. In de Haan (2011, Figure 7) we noted that, after quality control and smoothing, the derived ambient temperature from a single aircraft profile may also locate temperature inversions. However, de Haan (2011); Mirza *et al.* (2016); Mirza (2017, table 6.2)

2

and Stone (2017) suggest that the uncertainty in the derived temperature from a single aircraft at low levels can range between 2 K and 10 K. This degree of uncertainty makes it difficult to locate the height and magnitude of the temperature inversion.

Stone and Kitchen (2015) showed that a mean temperature for a layer of thickness 2000 m could be computed using the global navigation satellite system's altitude reported by an aircraft's automatic dependent surveillance-broadcast (ADS-B) system. However, this method for determining thickness temperature is too coarse to resolve a temperature inversion.

All these methods use Mode-S/ADS-B reports from single aircraft to obtain temperature observations. In our new work, we investigate the usefulness of using all available Mode-S EHS reports from multiple aircraft to estimate a vertical temperature profile.

In section 2 the current methods for obtaining in situ temperature measurements are described. Section 3 describes the method used to collect Mode-S EHS reports, how the Mach temperature observation is derived, and how these are aggregated to form a mean temperature observation. Section 4 defines four smoothing filters used to reduce the variance in Mode-S EHS reports. These are centred moving average, block average, linear regression and irregular exponential smoothing. In section 5 we apply the method described in section 3 to a case study based around London Heathrow to indicate the presence of temperature inversions. In section 6 we apply the four low-pass filters, to a sample of the data for the London Heathrow domain. In section 7 we show that the aggregated mean temperature profiles may provide useful information for operational meteorology, at least until temperature reports by ADS-B become more routinely available (RTCA, 2012). All times are expressed as Universal Time Coordinated (UTC).

2   In situ Upper Air Temperature Observations.

In situ observations of upper air temperature are made using a temperature sensor fixed to a device which ascends or descends between the surface and the top of the troposphere or beyond. Two types of such devices are the radiosonde and commercial aircraft.

For operational meteorology, modern radiosondes sample the atmosphere every second during ascent (World Meteorological Organisation, 2014, Ch 12, p.348), which can take up to two hours. Typically, radiosondes are launched from fixed sites that are widely separated (approximately 100 km) and report at fixed times (usually 0000 and 1200 UTC) so do not provide sufficient horizontal spatial or temporal resolution to capture the onset or duration of a temperature inversion (Fowler, 2010).

The common method of receiving observations from commercial aircraft is from the Aircraft Meteorological Data Relay (AMDAR) program. An AMDAR equipped aircraft reports the horizontal wind and ambient temperature obtained from the aircraft's flight management system (Painting, 2003). These reports are compiled on-board the aircraft and are transmitted to a ground station. The frequency of transmission depends on the phase of flight (and whether the aircraft is configured to send a report). For example, an aircraft may be configured to report every 6 seconds for the first 90 seconds during ascent then every 20 seconds until level flight; during level-flight reports are every 3 to 10 minutes; during descent reports are every 60 seconds (Painting, 2003, p.32).

In Europe, the AMDAR program is managed by E-AMDAR which provides at least one vertical profile once every three hours to participating National Meteorological Services (NMS) from around 100 airports across Europe. The Met Office obtains one vertical profile once every hour at major airports. In Europe and the UK, the reporting frequency of vertical profiles depends on the financial resources made available by the NMS. This contrasts with Air Traffic Management (ATM) which can interrogate an aircraft's transponder at a much higher frequency from a ground station SSR.

3 Aggregation of Mode-S EHS Reports.

Mode-S EHS is used by ATM to retrieve routine reports on an aircraft's state vector at a high temporal frequency (every 4 to 12 seconds). The aircraft's state vector consists of true-airspeed (hereafter referred to as the airpseed), magnetic-heading, ground speed, ground heading, altitude and Mach number. These Mode-S EHS reports can be used to derive estimates of the ambient air temperature and horizontal wind at the aircraft's location (de Haan, 2011).

During the study period, the Met Office used a Mode-S EHS receiver network which consists of five receivers (Stone and Pearce, 2016). Reports that are actively polled for by ATM and those routinely broadcast by aircraft are collected and processed by the Met Office receiver network.

The Met Office Mode-S EHS receivers are co-located at sites used for the weather radar network, which provide a good line of sight of aircraft flying above 500 m, power supply and communication network. The Mode-S EHS reports are collated then transmitted in batches every 10 minutes to a central processing facility, where the data are then passed through a quality control process (Stone and Pearce, 2016; Mirza, 2017). However, this network of Mode-S EHS receivers may be sub-optimal for the acquisition of Mode-S EHS reports at low levels,

Figure 1: Spatial distribution of trajectories (circles, colour-coded by altitude) for ascending and descending aircraft within the London Heathrow domain, derived from Mode-S EHS reports received between 1200 to 1300 on 4 January 2015. The domain extends for a distance of 80 km east-west, 40 km north-south, height 3000 m from the surface, with London Heathrow airport at the domain's centre. Points where the aircraft's roll angle is greater than 5°, i.e. when turning, are removed since these data are considered unreliable. (Cartography ©OpenStreetMap contributors, licensed as CC BY-SA https://www.openstreetmap.org/copyright, 2018)

e.g., below 500 m, due to loss of the line of sight required to receive Mode-S EHS reports.

Figures 1 and 8 (see supplementary section) show the distribution of the Mode-S EHS reports received from the Met Office Mode-S EHS receivers for a domain centred around London Heathrow airport. The domain's dimensions are sufficient to contain the trajectories of aircraft arriving at or departing from London Heathrow. Trajectories for descending aircraft are longer than for ascending aircraft. The domain excludes the areas where aircraft are held prior to their descent. The domain is not cuboid but can be imagined as an inverted truncated pyramid, centred at the airport. (In the supplementary section, figure 9 shows the distribution of Mode-S EHS reports for a domain centred around London Gatwick airport.)

5

The Mach Temperature, T_{MACH}, is derived from Mode-S EHS reports of Mach number, M and airspeed, V_A, (de Haan, 2011; Mirza *et al.*, 2016), such that

$$T_{\text{MACH}} = \frac{T_0}{A_0^2} \left[\frac{V_A}{M} \right]^2 , \tag{1}$$

where the speed-of-sound $A_0 = 340.294$ ms^{-1} and the assumed surface temperature $T_0 = 288.15$ K, are reference values defined at mean-sea-level pressure under international standard atmosphere conditions (ICAO, 1993).

To use as many of the Mode-S EHS reported data as possible they are aggregated to form a mean Mach Temperature, $\overline{T}_{\text{MACH}}$, observation. This 'aggregated observation' (Mirza *et al.*, 2016; Mirza, 2017, Ch3) is the arithmetic mean of all the Mach Temperatures, derived using equation (1), for all Mode-S EHS reports received within a defined time period and in a specified horizontal layer. The assigned position of $\overline{T}_{\text{MACH}}$ is set at the centre of the horizontal layer and at the mean pressure altitude of all the reporting aircraft within. These layers form a vertical profile of $\overline{T}_{\text{MACH}}$ observations when stacked in the vertical, which is centred around an airport.

We treat the errors as random so that the aggregated observation has a smaller error than an individual observation, since if the errors are random and uncorrelated then the standard error of the mean scales by $1/\sqrt{n}$, where n is the number of reports (Hoel, 1984, Ch 5 and Ch 10).

4   Temporal smoothing using low-pass filters

Studies by de Haan (2011); Mirza *et al.* (2016) have shown that Mach number and airspeed in equation (1) are subject to fluctuations which result in unrealistic values of derived temperature. These fluctuations are thought to arise as a result of the reduced precision of these data caused by the Mode-S EHS transponder processing the data prior to its transmission. De Haan (2011) showed that by applying a linear smoothing algorithm to the time series of Mode-S EHS reported Mach number and airspeed of a single aircraft before computing the derived Mach Temperature then the large fluctuations in the latter are reduced. This action of linear smoothing is similar to that of a low-pass filter, which reduces high-frequency components of a time-varying signal. We apply and evaluate a selection of low-pass filters.

The low-pass filters described in this section are applied to the time series of Mode-S EHS reports for each aircraft trajectory and the result of the low-pass filter is used to generate a

152 new aircraft report. Using this filtered time series of reports the Mach Temperature report is
153 recomputed.

154 In our description of the filters, we use the notation x_k, for the value of an individual Mode-S
155 EHS report, with assigned time t_k. The filtered reports, $X_{\bar{t}}$, are computed by averaging over a
156 validation window of length W_L, and they are assigned a validity time, $\bar{t}$.

4.1 Block-window average (BLK)

The block-window average method creates a time series of Mode-S EHS reports using the
average of all reports within a validation window, of length W_L. The time series is split into a
sequence of non-overlapping blocks then the average of each block is computed. In computing
the average no report is used more than once. The newly filtered time series is given by,

$$X_{\bar{t}} = \frac{1}{2m+1} \sum_{j=-m}^{+m} x_{k+j} \quad \text{for } k = m+1, 3m+2, 5m+3, ..., \left\lfloor \frac{N}{2m+1} \right\rfloor (2m+1) - m, \quad (2)$$

where N is the total number of reports in the time series and $\left\lfloor \frac{N}{2m+1} \right\rfloor$ is the number of validation
windows of length $W_L = 2m+1$ in the dataset. (The floor operator $\lfloor z \rfloor$, gives the greatest
integer that is less than or equal to z (Oldham *et al.*, 2010, p.68).) The validity time, $\bar{t}$, is given
by,

$$\bar{t} = \frac{1}{2m+1} \sum_{j=-m}^{+m} t_{k+j}. \quad (3)$$

158 This method is simple to implement but is not robust. It is susceptible to large variations since
159 all the reports within the validation window are equally weighted.

4.2 Centred moving average (CMA)

161 This is a straightforward method of computing a value over a short window length, $W_L = $
162 $2m+1$. This method is also known by other names, e.g., running-mean, running-average,
163 sliding-window average. Our method uses m reports before and after the current report, which
164 is at the centre of the window. Each report is weighted equally, so reports from the start to
165 the end of the window are treated to be of the same importance (Savitzky and Golay, 1964;
166 Wendisch and Brenguier, 2013). The new time series is given by,

$$X_{\bar{t}} = \frac{1}{2m+1} \sum_{j=-m}^{+m} x_{k+j} \quad \text{for } k = m+1, m+2, m+3, ..., N-m, \quad (4)$$

7

167 with the validity time given by eq. (3).

168 However, this method is also not robust since it can be affected by large outliers, and fluctua-
169 tions in the new time series may lag behind those seen in the original time series, although the
170 magnitude of the variations is reduced.

4.3 Piece-wise linear regression (LIN)

171

This uses the least squares regression method to compute a local rate of change, which is
assumed to be linear over the validation window, W_L. In other words, the mean values obtained
from fitting a straight line to the data locally are used to create the new time series. This is
a statistical method that minimises the differences between a control variable and predicted
values. The new time series is given by

$$X_{\bar{t}} = \alpha \bar{t} + \beta, \tag{5}$$

where the validity time is given by eq. (3). The local constant, β, is defined as

$$\beta = \overline{x} - \alpha \bar{t}. \tag{6}$$

where

$$\overline{x} = \frac{1}{2m+1} \sum_{j=-m}^{+m} x_{k+j}, \text{ for } k = m+1, m+2, m+3, ..., N-m, \tag{7}$$

i.e., the local mean $\overline{x}$ computed over the window. The corresponding local rate of change, α,
(i.e., the gradient) is given by,

$$\alpha = \frac{\sum_{j=-m}^{+m}(x_{k+j} - \overline{x})(t_{k+j} - \bar{t})}{\sum_{j=-m}^{+m}(t_{k+j} - \bar{t})^2}. \tag{8}$$

172 Unlike the centred moving average this method is more responsive to variations in the time
173 series.

4.4 Irregular exponential moving average (IRR)

174

175 The exponential smoothing method is similar to the centred moving average except observa-
176 tions are weighted according to their position in time. The current observation is weighted more
177 than the observations made at earlier times. The simple exponential moving average (Brown,
178 2004; Kim and Huh, 2011) assumes observations are available at regular time intervals. How-

ever, since the Mode-S EHS reports used to construct aircraft trajectories may be at irregular time intervals and there may be missing data, the Wright (1986) method is used, which extends the exponential smoothing method to irregular time intervals. The new time series is given by,

$$X_{t_k} = (1 - V_k)X_{t_k-1} + V_k x_{t_k}, \tag{9}$$

where

$$V_k = \frac{V_{k-1}}{b_k + V_{k-1}} \tag{10}$$

and

$$b_k = (1 - a)^{(t_k - t_{k-1})}, \tag{11}$$

for $k = 2, 3, 4, ...N$, and $0 \leq a < 1$.

The value a is a smoothing parameter which determines the proportion of the new information to be added to the running average. The parameter V_k is a weighting function which is given an initial value of $V_1 = 1$. The larger the value of the parameter V_k, the less weight is given to the running average. The weighting function depends on the time separation between reports. For each X_{t_k} the assigned validity time is t_k since the former directly replaces each x_{t_k}.

4.5 Consistency check

We apply a consistency check so that the horizontal spatial and temporal resolutions of the time series are reasonably consistent along the aircraft trajectory. This consistency check is applied because there are fewer Mode-S EHS reports along an aircraft's trajectory than are actually available in principle.

We assume that a break in the time series of reports arise as a result of either (a) the aircraft exiting from a turning point on its approach to land, (b) that it passed out of then re-entered the airport domain, shown in figure 1, (c) that the aircraft was not within the line of sight reception to the Mode-S EHS receiver or (d) due to quality control pre-processing of Mode-S EHS reports, performed at the monitoring site (Stone and Pearce, 2016), which removes reports when an aircraft's roll angle exceeds 5 degrees creating gaps in the time series of reports.

The consistency check is used to determine when a low-pass filter outputs a filtered value. The filtered value $X_{\bar{t}}$ is set to a missing data indicator when the time difference between two successive reports, δt, used to compute the filtered value is greater than a maximum permitted time difference, $\delta t > \delta t_{max}$. (This affects the BLK low-pass filter more as reports are only used once.) The value of δt_{max} ensures that the data input to the low-pass filter are closely

related in time and space.

We select a value for δt_{max} equal to the standard deviation of the time difference between successive Mode-S EHS reports along an aircraft's trajectory. For the selected day we use all aircraft trajectories to compute this standard deviation. The result is rounded to the nearest whole second.

The effect of applying the consistency check is to set the maximum time window for sampling the meteorological conditions based on the validation window of length W_L.

5 Inversion Case Study

In this section, we use a case study to identify useful meteorological information for the London Heathrow domain between 4 and 5 January 2015. This period was chosen because fog was a persistent weather feature. One of the meteorological conditions for fog to arise is the presence of a temperature inversion at low altitude or near the surface.

5.1 Observations

To assess the information content of the $\overline{T}_{\mathrm{MACH}}$ vertical profile we compare it to temperature reports from other observation systems. We use the high-resolution temperature profile from Herstmonceux, the nearest radiosonde station. We also use AMDAR temperature reports. We note also that all AMDAR reporting aircraft also report Mode-S EHS. We assume that radiosonde and AMDAR observations are representative of the meteorological conditions. The vertical profile of $\overline{T}_{\mathrm{MACH}}$ is compared to the forecast mean vertical temperature profile from the Met Office's limited-area, high-resolution, convection-permitting NWP model for the United Kingdom, the UKV (Lean *et al.*, 2008; Tang *et al.*, 2013); the mean is calculated using UKV vertical profiles at selected points across the London Heathrow domain. We note that the radiosonde and AMDAR temperature reports that we use for comparison are not assimilated by the UKV.

In figure 2 we show all temperature reports for the London Heathrow domain on 4 January 2015 with a validity time of 0600, that is all observations received between 0530 and 0630. The $\overline{T}_{\mathrm{MACH}}$ profile (black triangles) is constructed using the aggregation method described in section 3. The $\overline{T}_{\mathrm{MACH}}$ error bars (black) are the 95% confidence limits for the mean using the Student-t distribution (Hoel, 1984, Ch 5 and Ch 11). For comparison, we show in situ observations from two other observing systems: radiosonde and AMDAR. The radiosonde was launched at 0515, headed due south of its launch site at Herstmonceux and reached an altitude
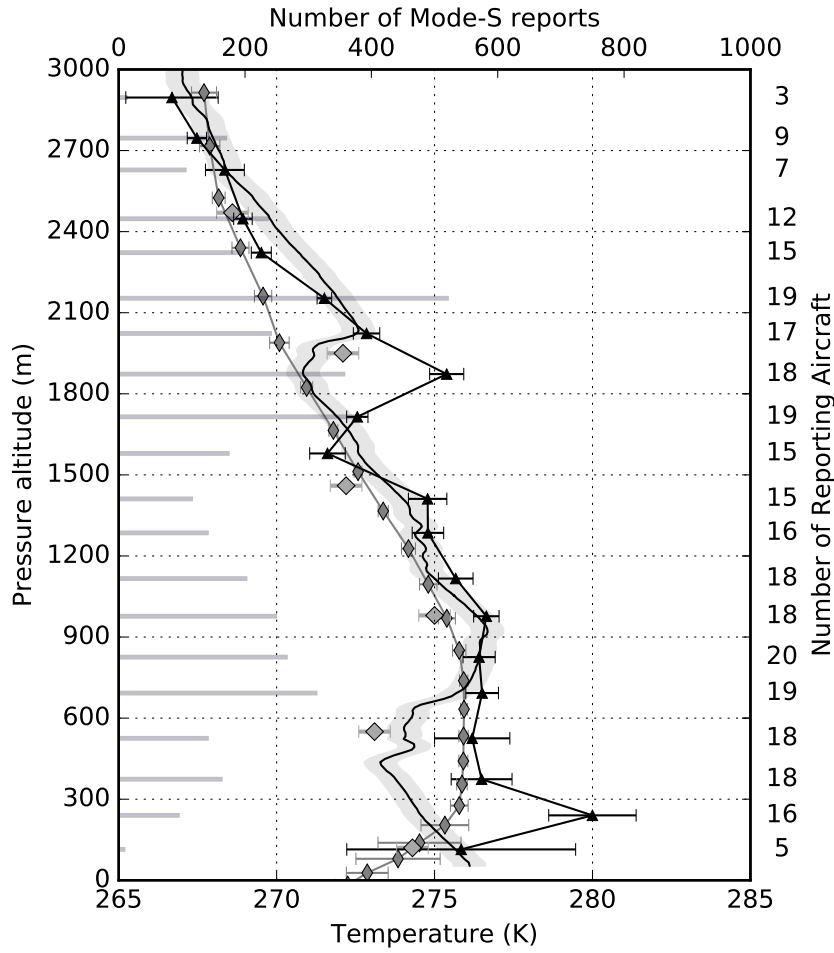
10

Figure 2: Temperature reports for the London Heathrow domain on 4 January 2015 for the period 0530 to 0630. Aggregated Mach Temperature observation and its 95% confidence interval (black triangles), with the number of Mode-S EHS reports used shown by the horizontal bars from the left, and the number of reporting aircraft shown on the right-axis. Herstmonceux radiosonde report valid at 0600 (black solid line, with its reported precision of ± 0.5 K shown by the grey shading), AMDAR reports (large diamonds) and their reported precision of ± 0.5 K (error bars), and the mean UKV forecast and its 95% confidence interval, valid at 0600 from the forecast run at 0300 4 January 2015 (narrow diamonds).

of 3000 m at 0524. Position and temperature reports were made every 2 s. The region of the atmosphere sampled by the radiosonde is not contained within the London Heathrow domain. AMDAR temperature reports are shown as point observations (Painting, 2003), received between 0557 and 0617 from an aircraft destined to land at London Heathrow during this period. We also show the mean UKV forecast temperature profile for the London Heathrow domain

with the validity time 0600. The mean forecast temperature profile is computed by using a sample of nine 1-D column profiles from across the London Heathrow domain (Mirza, 2017, Fig 5.5). The standard deviation of the mean forecast temperature profile indicates that at this time between the pressure altitude range 300 m and 3000 m there is little variation across the domain (<0.5 K) and below 300 m it is around 1.5 K. (For this pressure altitude range Ingleby and Edwards (2014) estimated that the average UKV model error to be ± 0.75 K when compared against high-resolution radiosonde reports.)

5.2 Observed Meteorological Features

In figure 2 the radiosonde report indicates the presence of two temperature inversions: a low-level temperature inversion between 500 m and 900 m, reported at 0516, and an elevated temperature inversion between 1800 m and 2000 m, reported at 0520. The AMDAR observations, reported between 0557 and 0612, are broadly in agreement with the radiosonde. These in situ observations provide a broad description of the vertical temperature structure of the atmosphere between Heathrow airport and Herstmonceux. However, there is a clear difference between these in situ observations and the mean UKV forecast for the London Heathrow domain.

The UKV at 0600 forecasts a low-level inversion between the surface and 300 m but does not forecast the elevated inversion between 1800 m and 2000 m. However, the $\overline{T}_{\mathrm{MACH}}$ observations, obtained between 0530 and 0630, do suggest that an elevated inversion is present.

The radiosonde and AMDAR reports were not included in the UKV analysis (i.e., the initial state of the NWP model) as they were received after the data assimilation observation processing period, 0130 to 0419. Therefore the UKV forecast will not have taken into account the existence and the location of the temperature inversions shown by these observations and there are no other sources of in situ upper air temperature observations during the observation processing period. Furthermore, the elevated temperature inversion is not forecast by the UKV at 0300, 0400 and 0500 within the London Heathrow domain, but this may also be due to deficiencies in the physical modelling within the UKV.

The $\overline{T}_{\mathrm{MACH}}$ observations appear consistent with the radiosonde and AMDAR reports between 700 m and 3000 m. In this case, while there are insufficient AMDAR reports to resolve the inversion, its presence is shown by the $\overline{T}_{\mathrm{MACH}}$ observations at around 1900 m, even though the magnitude of the inversion suggested by the $\overline{T}_{\mathrm{MACH}}$ report differs significantly from that shown by the radiosonde. The radiosonde and AMDAR show the inversion to be higher, but this difference could be accounted for by a horizontal variation in the inversion height. Below 700 m the $\overline{T}_{\mathrm{MACH}}$ observations are more consistent with the UKV forecast, except around

12

300 m, where the difference between the UKV and $\overline{T}_{\text{MACH}}$ is of the same magnitude as at 2000 m, i.e., approximately 5 K.

The absence of the elevated temperature inversion at around 2000 m in the UKV forecast would be important for the subsequent forecasts of other meteorological phenomena. An elevated inversion in effect caps vertical movement and dispersion of atmospheric aerosols. This may affect the forecast conditions for solar insolation and the formation or persistence of fog and cloud (Fowler *et al.*, 2011). We suggest that $\overline{T}_{\text{MACH}}$ observations could provide an additional source of information, albeit a qualitative source, on the vertical temperature profile that may otherwise be unknown, since the 0600 Herstmonceux radiosonde report is made only on demand (unlike the reports at 0000 and 1200). We illustrate the qualitative information contained in the $\overline{T}_{\text{MACH}}$ observations in figure 3.

Figure 3 shows the temperature reports available for the validity time 0900 on 4 January 2015; these are all reports received between 0830 and 0930. There are no in situ observations from radiosonde because there is no routine launch at this time of day. The 13 AMDAR observations were reported between 0830 to 0837 from an aircraft on a descent path to Heathrow airport. The computation and depiction of the $\overline{T}_{\text{MACH}}$ observations and UKV vertical temperature profile are as described in figure 2. We note that $\overline{T}_{\text{MACH}}$ observations suggest that the elevated inversion noted in figure 2 still persists although at a lower altitude, between 1500 m and 1800 m, with a broadly isothermal region between 1000 m and 1500 m. The AMDAR reports are broadly in agreement with the presence of the temperature inversion but not with the isothermal region. The UKV forecast for these two regions does not show either meteorological feature. The AMDAR reports would not have been available for assimilation into the UKV. Figure 4 shows the same time period but 24 hours later for which there are no AMDAR or radiosonde reports. In this case, the UKV forecast and the $\overline{T}_{\text{MACH}}$ observations show some agreement indicating the presence of an elevated temperature inversion between 1000 m and 1500 m. Thus, in the absence of other in-situ observations, the $\overline{T}_{\text{MACH}}$ observations could provide useful information about the vertical structure of the atmospheric temperature.

Figures 2, 3 and 4 all show that $\overline{T}_{\text{MACH}}$ indicates warmer conditions compared to the UKV forecast. This may be due to a bias in $\overline{T}_{\text{MACH}}$ resulting from the numbers of aircraft that are ascending and descending at any given time (although it is also possible that the UKV NWP model is biased). Studies by Mirza (2017) and Stone (2017) suggest that $\overline{T}_{\text{MACH}}$ reports between the surface and 3000 m appear cooler than the ambient conditions when aircraft ascend, while for descents these reports appear warmer. These effects may be the result of aircraft manoeuvrings during ascent or descent. For example, most descending aircraft extend their
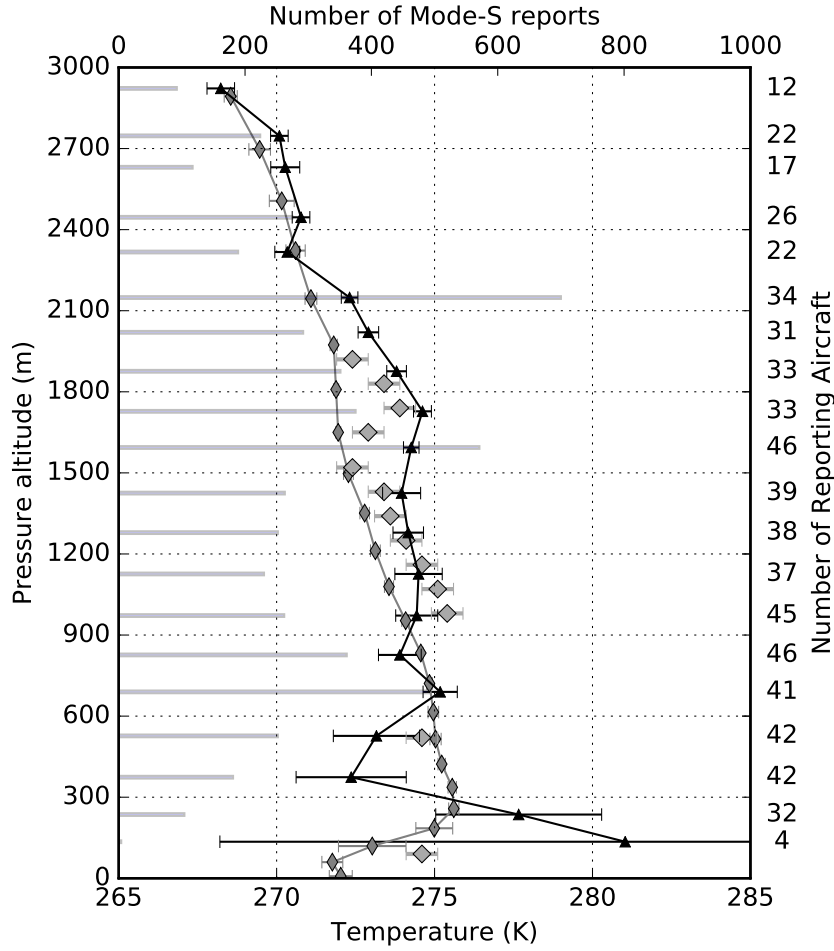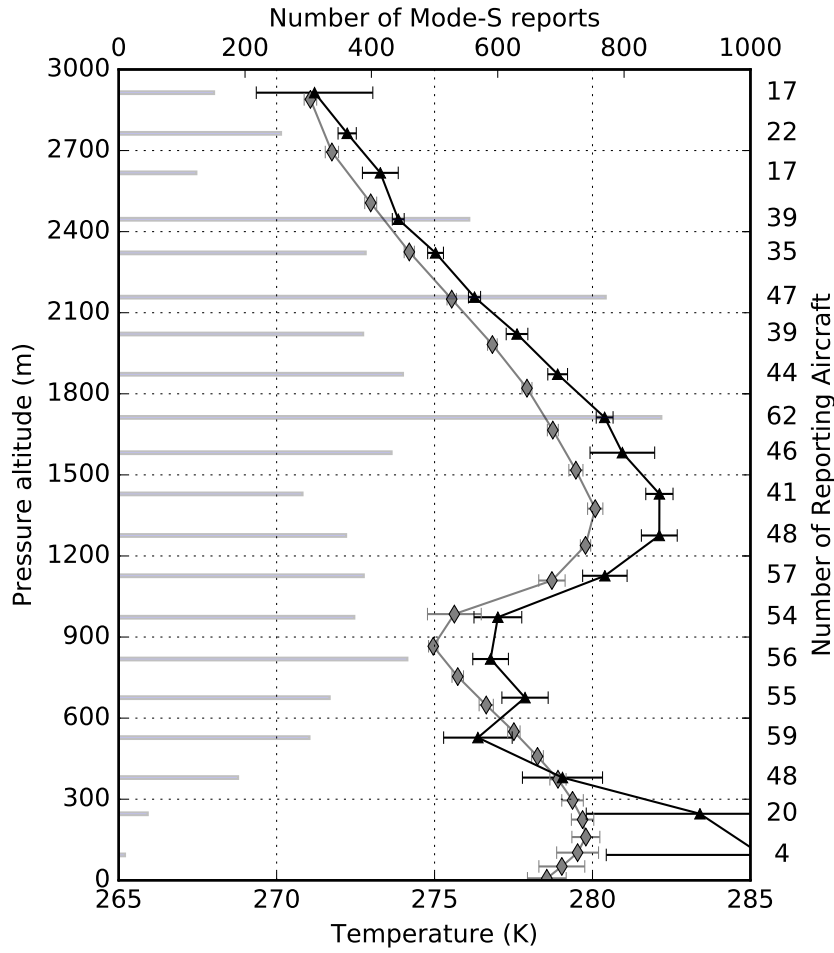
13

Figure 3: Temperature reports for the London Heathrow domain on 4 January 2015 for the period 0830 to 0930. Symbols are as described in figure 2. This plot shows the aggregated Mach Temperature reports and the corresponding number of Mode-S EHS reports, AMDAR reports, and the mean UKV forecast valid at 0900 .

landing gear and set full flaps at a height of around 300 m. This causes a strong deceleration, which could explain major deviations of the reported Mach number from the observed airspeed and thus erroneous temperatures. In addition, the height where the $\overline{T}_{\text{MACH}}$ profile deviates from the other data coincides with the bottom (and the most probably populated) level of London Heathrow's holding patterns at 2000 m. Aircraft on hold do significantly more manoeuvring which may lead to a decrease in the accuracy of the derived T_{MACH} reports. Mirza *et al.* (2016, Figure 11) suggest that with sufficient Mode-S EHS reports from a single aircraft type, e.g., greater than 100 at each altitude interval, then any bias may be reduced to near zero. However, Stone (2017, Figure 1b) suggests that the bias may depend on whether the aircraft is ascending
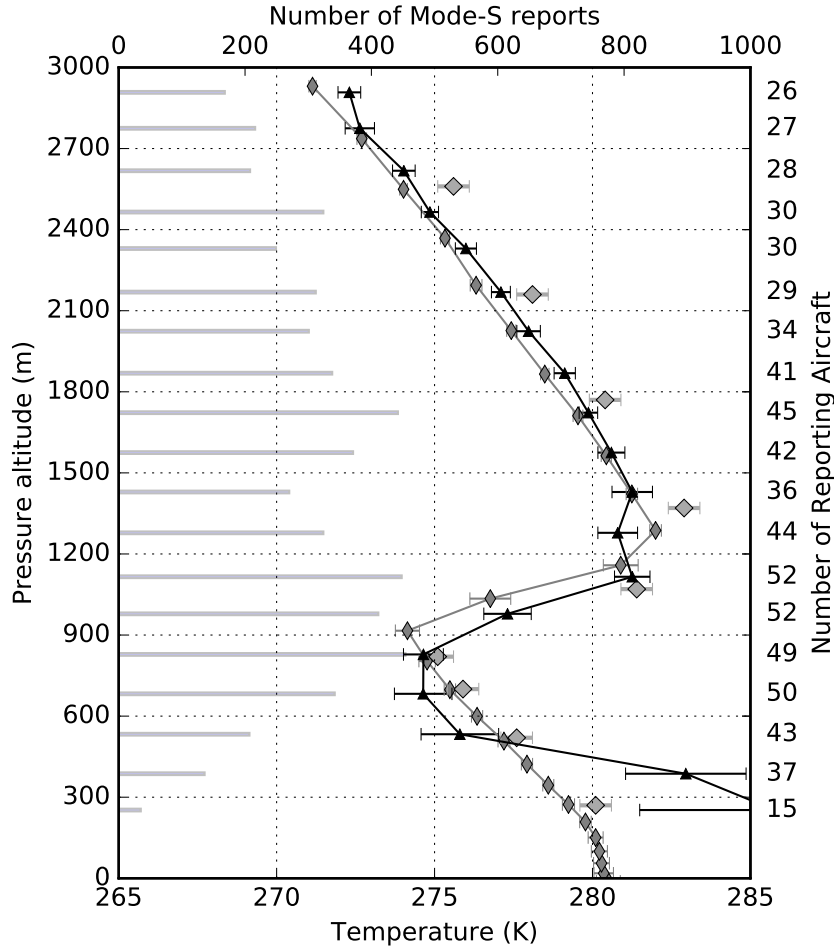
14

Figure 4: Temperature reports for the London Heathrow domain on 5 January 2015 for the period 0830 to 0930. Symbols are as described in figure 2. This plot shows the aggregated Mach Temperature reports and the corresponding number of Mode-S EHS reports and the mean UKV forecast valid at 0900. The lowest two points (not shown) are 283.4±3.6 K and 285.3±4.9 K. There were no radiosonde or AMDAR reports available for this time period and altitude range.

316 or descending. Further research is needed to understand these effects, for example. a much
317 longer study such as was done for AMDAR (Drue *et al.*, 2008).

318 Figure 5 shows similar temperature reports as shown in figure 4 but for the validity time at
319 2100 on 5 January 2015; these are all reports received between 2030 and 2130. There are no
320 radiosonde observations, but there were 9 AMDAR reports received between 2043 and 2045
321 from an aircraft departing from Heathrow. The UKV mean profile is for 2100 from the forecast
322 run at 2100 on 5 January 2015, so this represents the NWP analysis. Unlike the previous

15

Figure 5: Temperature reports for the London Heathrow domain on 5 January 2015 for the period 2030 to 2130. Symbols are as described in figure 2. This plot shows the aggregated Mach Temperature reports and the corresponding number of Mode-S EHS reports, available AMDAR reports and the mean UKV forecast valid at 2100 from forecast run at 2100 on 5 January 2015. The lowest two points (not shown) are 283.0±1.9 K and 285.8±4.3 K. There were no radiosonde reports available for this time period and altitude range.

examples, it is likely that the AMDAR reports were received in time for their assimilation prior to the UKV forecast run. Therefore there is a good correspondence between the AMDAR temperature reports and UKV mean temperature profile. The $\overline{T}_{\mathrm{MACH}}$ observations between 600 m and 3000 m also show a good correspondence, in particular capturing the elevated inversion between 900 m and 1500 m. However, in each of the cases shown, at or below 1000 m the $\overline{T}_{\mathrm{MACH}}$ observations show increased level of uncertainty, as shown by the 95% confidence limits, and large differences between the AMDAR and radiosonde observations,

and the UKV forecasts.

The radiosonde and AMDAR reports are effectively instantaneous values, reporting on a time scale of seconds to minutes. The $\overline{T}_{\mathrm{MACH}}$ observation uses all available Mode-S EHS reports over a large spatial domain, and is an average over the hour thus representing the mean conditions in space and time. The horizontal bars shown in figure 2 indicate the number of observations used to compute each $\overline{T}_{\mathrm{MACH}}$ observation. The mean time difference between reports is 2 seconds per aircraft which corresponds to a horizontal spatial sampling scale around 250 m, however, any variability on this scale will be lost due to the averaging process. Where there is an agreement between the $\overline{T}_{\mathrm{MACH}}$ observation and the UKV this may be due to the latter also representing the mean conditions over the hour, although its spatial sampling scale is 1500 m.

We do note that $\overline{T}_{\mathrm{MACH}}$ observations show a degree of variability, as represented by the 95% confidence limits. The large variation in the computed $\overline{T}_{\mathrm{MACH}}$ observations may be due to the low precision of the underlying data, mainly the Mach number (de Haan, 2011; Mirza, 2017). The large uncertainty in the confidence limits is due to the drop in the available number of Mode-S EHS reports used to compute the $\overline{T}_{\mathrm{MACH}}$ observations. Using the Student-t distribution to compute the confidence limits may be unreliable or unsuitable at these low levels as the distribution of the individual T_{MACH} reports becomes multi-modal. Since the atmospheric conditions do not appear to vary greatly over the hour, we suggest that variability of $\overline{T}_{\mathrm{MACH}}$ observations is likely to be due to the precision of the Mode-S EHS data used to derive the Mach Temperature (Mirza *et al.*, 2016; Mirza, 2017). This results in the poor characterisation of the vertical temperature profile at levels below 1000 m. (Figures 10 and 11 in the supplementary section (available online) show examples of the derived profiles for a similar size domain with London Gatwick airport at its centre for the same case study period.)

This variability is not seen in the radiosonde and AMDAR reports, especially at levels below 1000 m. However, there are insufficient AMDAR reports to characterise fully the vertical temperature profile, and so they may not capture inversions between the surface and 600 m. The low reporting of AMDAR may be due to operational constraints, e.g., availability of suitably equipped aircraft or cost constraints which limit reporting to a single aircraft.

17

6 Temporal smoothing using low-pass filters

6.1 Motivation for low-pass filtering

In section 5.2 it was shown that T_{MACH} reports are subject to a high degree of variability especially at altitudes below 1000 m. De Haan (2011) and Mirza (2017) suggest the variability is due to the effects of Mode-S EHS processing. In this section, we apply four methods that perform the function of a low-pass filter, described in section 4, to a sample of the data for the London Heathrow domain. The filters are applied to the time series of Mode-S EHS reports for each aircraft within the London Heathrow domain. The filters create a new time series of smoothed Mode-S EHS reports which are then used to compute T_{MACH} observations (eq. (1)).

Figure 6 has four panels. Each panel shows the same short time series of non-smoothed Mode-S EHS reports (grey dots) for Mach number and airspeed, and over the period of one minute there are 28 reports of each. The corresponding derived Mach Temperature ranges between 269 K and 291 K. However, such a change in the ambient temperature in one minute is unrealistic. De Haan (2011) suggests that this magnitude of change in Mach Temperature is due to the low precision of the reported Mach number. Mirza (2017) shows that this is indeed the case but then goes on to suggest that the variation in Mach Temperature is also due to the asynchronous changes in the Mode-S EHS reports of Mach number and airspeed. Close examination of figure 6(a) shows the effects of low precision and asynchronous changes.

In figure 6(a)(i) the first six Mach number reports show there are two step changes of -0.004 while the airspeed remains constant, indicated by region A, figure 6(a)(ii). These step changes represent the reporting precision of the Mach number after Mode-S EHS processing. The corresponding Mach Temperature, figure 6(a)(iii), computed using equation (1), show step changes of +7 K. These changes occurred over 9 s with two step changes in altitude: 1821 m to 1814 m to 1806 m (not shown). Equation (1) suggests that if the airspeed is constant then a decrease in the Mach number corresponds to an increase in Mach Temperature. This is also suggested by figure 2 where for the altitude range of these Mode-S EHS reports the radiosonde and AMDAR reports indicate the presence of a temperature inversion.

In figure 6(a)(ii), the report at region B for airspeed shows a large step change of -8 knots while the Mach number and altitude are unchanged. This results in a step change of -21 K in the corresponding Mach Temperature in 1 s. Equation (1) suggests that if the Mach number is constant then a decrease in airspeed corresponds to a decrease in the Mach Temperature. However, for the 1 s over which this change takes place the aircraft's reported altitude remained at 1806 m and its horizontal displacement was 138 m. It is unlikely that the actual ambient

18

temperature would change by this magnitude over such a short distance and time. But if we assume that temperature is constant then equation (1) shows that a decrease in airspeed should show a corresponding decrease in Mach number, which in this instance did not occur. We suggest, therefore, that the Mode-S EHS processing causes asynchronous changes in the Mach number and airspeed which may result in the observed large fluctuations in Mach Temperature.

Regions C and D show a synchronous change in Mach number and airspeed, which results in a change of Mach Temperature of -9.5 K. The changes in altitude for each occurrence were 1783 m to 1768 m over 5 s and 1737 m to 1722 m over 4 s. We suggest that the change in magnitude, while smaller than for the asynchronous case at region B, is due to the Mode-S EHS processing which reduces the precision of the Mach number and airspeed.

In summary, there are two effects of Mode-S EHS processing that may account for the observed variability in the derived Mach Temperature: the reduced precision of the reported Mach number and airspeed and their asynchronous changes. The use of a suitable low-pass filter may smooth out the step changes in Mach number and airspeed thus reducing the observed variability in the derived Mach Temperature. We consider the use of low-pass filters in the next section.

6.2 Applying low-pass filters to time series of Mode-S EHS Reports

We now explain how we set-up and use the low-pass filters. For the London Heathrow domain, the consistency check δt_{max} is 6 s. For BLK (eq. (2)), CMA (eq. (4)) and LIN filters (eq. (5)) the validation window is set with $m = 2$. This provides five reports for the validation window, i.e., where each filtered report has two reports either side, which are used to compute the mean value, except at the start and end of the time series. If 6 s is the maximum time separation between the five reports within the validity window then the filtered report represents the meteorological conditions sampled over 30 s. This is an appropriate sample time given that aircraft are changing position horizontally and vertically. Typical ascent rates are 5-10 ms^{-1} so a 30 s averaging could be over 150-300 m in the vertical. This is similar to the vertical grid length in many NWP models. Typical glide speed would be 100-120 ms^{-1} giving a horizontal representation over 3.0-3.6 km. During the sampling time the aircraft may make control movements that increases or decreases its altitude during any part of its phase of flight: ascent, en-route or descent. These may be considered as an additional source of high-frequency noise.

There is a trade-off between the parameters δt_{max} and m. If δt_{max} is too short in time then high-frequency components may not be sufficiently damped. Furthermore, this limits the num-

ber of reports used due to failing the consistency check (see section 4.5). If the window length is too large then over-smoothing may result which may cause the position and altitude of the temperature inversion to be either misplaced or not detected. However, these parameters could be tuned for particular operational conditions at airports or to apply different consistency checks for ascending and descending aircraft since rates of ascent are larger than rates of descent. The additional outputs of these low-pass filters (except IRR) are the means of the time, latitude, longitude and pressure altitude quantities within the validation window.

For IRR (eq. (9)), we use a smoothing factor $a = 0.2$. The weighting function (eq. (11)) is initialised with the time difference $t_k - t_{k-1} = 1\ s$. These parameters were selected so that when the time separation between reports is $4\ s$, the expected SSR rotation rate, then the exponential smoothing will weight the previous filter value and the current observation equally. Thus the IRR low-pass filter replaces each Mode-S EHS report in the aircraft's trajectory, therefore, the low-pass-filtered trajectory contains the same number of reports.

6.3 Effect of applying low-pass filters

In figure 6 the resulting smoothed Mach number, airspeed and recomputed Mach temperature are shown as the square points after applying the low-pass-filters discussed in section 4. The main effect of the low-pass filters IRR, CMA, and LIN (figures 6(b), 6(c), 6(d) respectively) is to smooth the step transitions in Mach number and airspeed which reduces the variance of the Mach Temperature distributions at each altitude bin. This is the desired effect as it shows that the impact of the high-frequency components is being diminished.

We apply each of these low-pass filter methods to all aircraft trajectories within the London Heathrow domain. We then apply the aggregation method to recompute $\overline{T}_{\mathrm{MACH}}$ for each horizontal layer (shown in figure 2). Figure 7(a)(i) shows the results after applying the different low-pass filters. Figure 7(a)(ii) shows the difference between the smoothed and unsmoothed $\overline{T}_{\mathrm{MACH}}$ observations. Above 1000 m the difference ranges between ± 0.5 K. However, below 1000 m the magnitude of the smoothed $\overline{T}_{\mathrm{MACH}}$ is greater. The magnitude of the latter results may arise because reports have been filtered out during the low-pass filtering. This is shown in figure 7(b)(ii) where the number of reports for CMA and LIN are less than for IRR (the number of reports for the unsmoothed profile is the same as for the IRR). The number of reports for BLK low-pass filter is greatly reduced but this is expected since this method replaces a series of reports with a single report whereas the other low-pass methods use substitution. The overall effect of the applying the low-pass filters to the computed $\overline{T}_{\mathrm{MACH}}$ is minimal. However, the low-pass filters have a greater effect on the computed standard deviation of the $\overline{T}_{\mathrm{MACH}}$.
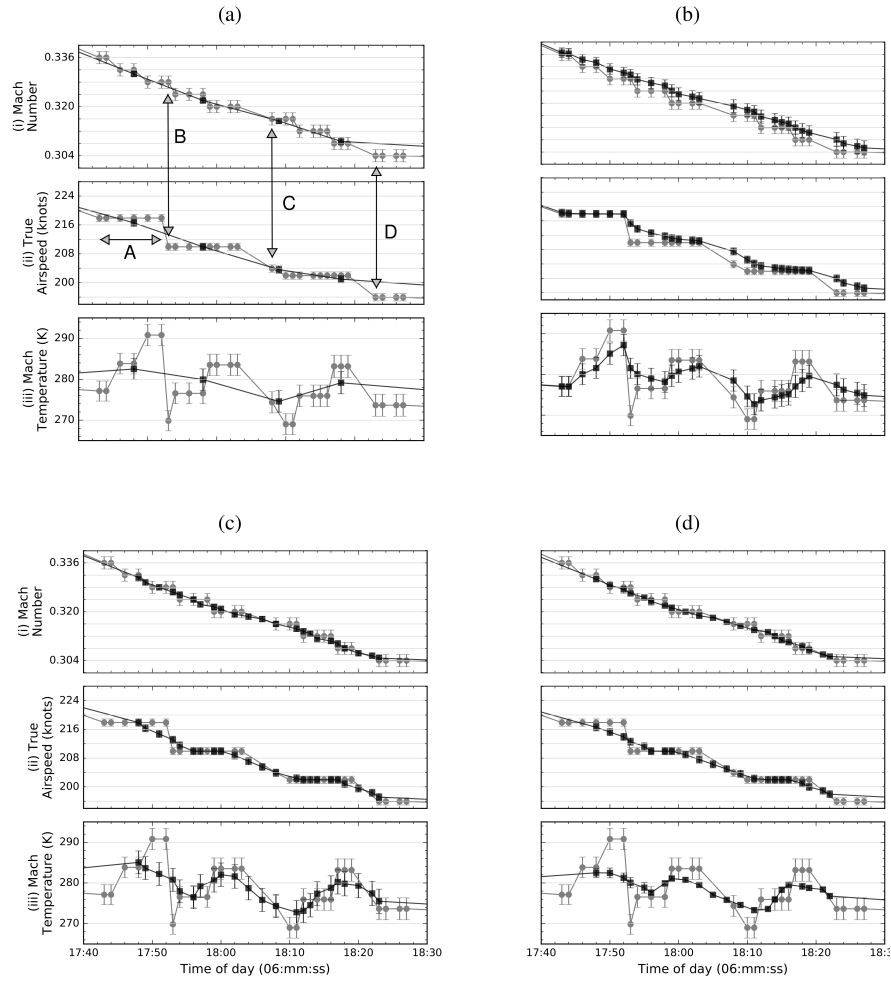
Figure 6: Before (circles) and after effects (squares) of applying smoothing filters for one aircraft's time series of (i) Mach number and (ii) true-airspeed for (a) Block Average, (b) Irregular Exponential, (c) Centred Moving Average and (d) Linear Regression. (iii) Mach Temperature computed before and after smoothing.
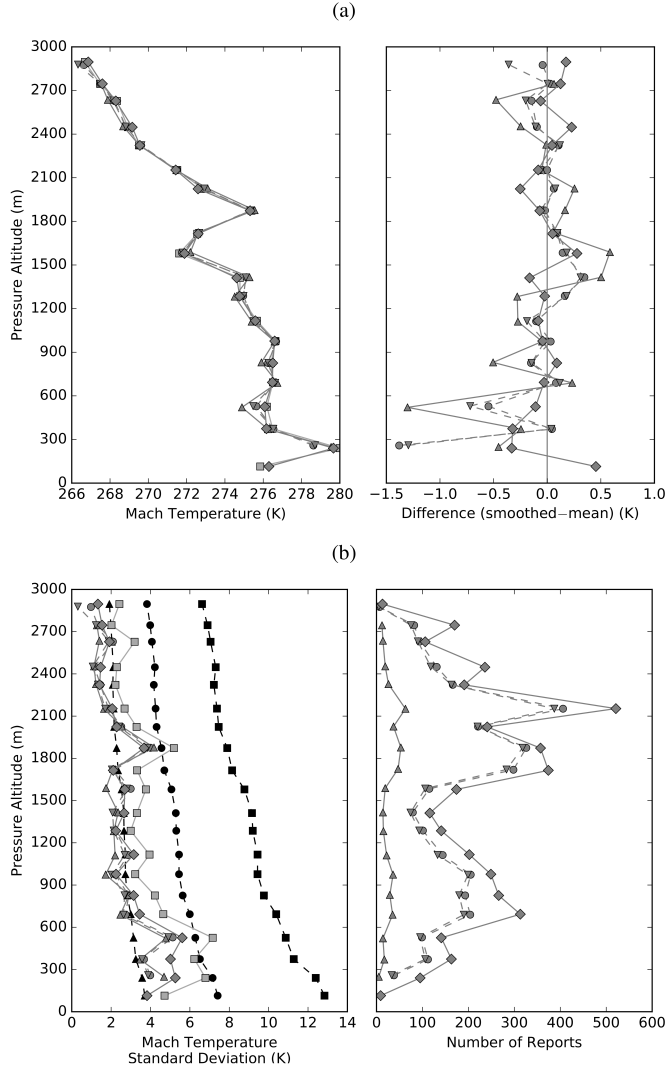
21

Figure 7: Effect of applying the different smoothing filters to Mode-S EHS reports of Mach number and true-airspeed along all aircraft tracks, London Heathrow domain, 4 January 2015 0530 to 0630. In each case (a) the resulting $\overline{T}_{\mathrm{MACH}}$ reports and (b) the estimated sample standard deviation are recomputed. Key: ■ uncorrected $\overline{T}_{\mathrm{MACH}}$, low-pass filtered: ▲ BLK, ● CMA, ▼, LIN, ◆ IRR. Estimated error:■ full precision, ● 2 × quantisation, ▲ quantisation.

Figure 7(b)(i) shows the effect of each low-pass filter on the computed standard deviation of the $\overline{T}_{\text{MACH}}$. For comparison also shown are the expected standard deviations for the $\overline{T}_{\text{MACH}}$, using the Mach Temperature error equation formulated by Mirza *et al.* (2016, Equation 16), assuming the following for the Mach number and airspeed: full precision error, precision due to quantisation error (Mirza *et al.*, 2016, figures 4 and 11) and precision due to double the quantisation error.

We used four low-pass filters: centred moving average (CMA), block average (BA), linear regression (LR) and irregular exponential smoothing (IRR). For smoothing the time series of reports above an altitude of 1000 m, the performance of each of the low-pass-filters was similar. Below 1000 m there was a small difference between using the moving window methods and the IRR. The former methods reduce variance more than the IRR. However, the advantage of the IRR method is that it uses all the available reports whereas the moving window methods removed reports as a result of the imposed quality control criterion. Furthermore, the IRR's weighting function is time-dependent, giving most weight to the most recent datum. This may reduce over-damping of high-frequency signals in the presence of a temperature inversion that would otherwise be smoothed by the moving window methods. However, each of the methods used to minimise the fluctuations in the Mode-S EHS derived observations, i.e., aggregation and low-pass filtering, effectively reduce the space and time resolution of the data.

7   Summary and Conclusions

This paper used Mode-S EHS reports exchanged between an aircraft and air traffic control to derive Mach Temperature. Using an aggregation of Mach Temperature reports from all aircraft within a defined region of an airport, e.g., the London Heathrow domain, vertical profiles of the mean Mach Temperatures, $\overline{T}_{\text{MACH}}$, for horizontal layers were constructed and used to identify a meteorological feature, temperature inversion, which is important for operational aviation weather forecasting and numerical weather prediction. To improve the representation of $\overline{T}_{\text{MACH}}$, low-pass filters were applied to the time series of Mode-S EHS reports of Mach number and airspeed for all aircraft within the London Heathrow domain. The low-pass filter smoothed the discrete transitions of the Mach number and airspeed, which occur due to their low precision. Anomalous values of the derived Mach Temperature, which arise due to the asynchronous change between the Mach number and airspeed, were also smoothed. The overall effect of the low-pass filter reduced the variance of the $\overline{T}_{\text{MACH}}$ by as much as 50%.

We compared hourly $\overline{T}_{\text{MACH}}$ profiles with in situ observations of temperature reported by radiosonde and AMDAR, when available. We found that the $\overline{T}_{\text{MACH}}$ profile between 1000 m and

23

3000 m shows some agreement with these in situ observations whereas below 1000 m there was less agreement, where the magnitude of the difference between the in situ observations and the $\overline{T}_{\mathrm{MACH}}$ was as great as 6 K. In our comparisons (figures 2, 3,4 and S3), $\overline{T}_{\mathrm{MACH}}$ seems to be in reasonable agreement with AMDAR and radiosonde data down to 600-700 m, a little lower than the 1000 m limit that we conservatively estimated. However, the results also show that some significant deviations can occur between 600 m and 1000 m. These arise in the early morning and the late evening, when there are few aircraft and so fewer Mode-S EHS reports at the lower levels. This scarcity may be due to the interruption of the line of sight between the aircraft and the Mode-S EHS receiver station. Hence we chose 1000 m as a safe lower limit for practical application. Daily operations may achieve better but this is best left to the meteorologist's judgement as they gain experience with the application.

However, the comparison against in situ observations is difficult since these are point based values, measured on time-scales of seconds to minutes, compared with the hourly mean of the aggregated Mach Temperature. Moreover, the radiosonde observations are not located within the airport domains. The temperature differences observed below 1000 m are unlikely to be due to changes in the ambient temperature; nor the prevailing meteorological conditions at the surface on the day (near freezing conditions, low wind speed and fog) but more likely due to Mode-S EHS processing (de Haan, 2011; Mirza *et al.*, 2016; Mirza, 2017; Stone, 2017).

We also compared the hourly aggregated Mach Temperature against the UKV model forecasts. We found similar results to our comparison with in situ observations. Furthermore, we found that the Mach Temperature profiles identified regions where temperature inversions may be present but which were not present in the UKV forecast, thus showing that Mach Temperature profiles may provide additional information for use in NWP.

From analysing the time series of the Mode-S EHS reports, we found that the Mode-S EHS processing also results in step changes in the reports of Mach number and airspeed that are asynchronous in time. This results in very large fluctuations in the corresponding Mach Temperature, ranging from 5 K to 9 K between adjacent reports.

We conclude that applying a low-pass filter to the time series reports of Mach number and airspeed could be beneficial as a pre-processing step prior to NWP data assimilation but further research would be needed in order to tune the filter parameters. Moreover, the IRR method could be used as the basis for a Kalman filter. While the quantitative value of the mean Mach Temperature may have a large uncertainty, the qualitative value of the constructed vertical profile of the mean Mach Temperature may provide additional information that may be useful for operational meteorology, e.g., identifying the possible locations for the occurrence of tempera-

ture inversions, when combined with other available sources of information. Furthermore, this may help aviation meteorologists to improve their forecasts for ATM by verifying in near-real-time the performance of the NWP forecast. However, further studies should be undertaken to assess this aspect.

The most common Mode-S EHS report is the aircraft's state vector from which temperature and horizontal wind observations can be derived. However, an alternative to Mode-S EHS is Mode-S MRAR (Strajnar, 2012; Strajnar *et al*., 2015), but the current regulatory environment does not require aircraft or ATM to make such reports available. The technology and capability already exist for the direct reporting by aircraft of the temperature and horizontal wind. There-fore, in the interest of making more effective use of aircraft based observations for operational meteorology and numerical weather prediction, the aviation industry should be encouraged to implement either Mode-S MRAR reporting or its planned successor ADS-B.

Acknowledgement

Supplementary Section.

In this supplementary section, in figures 8 and 9 we show for comparison the spatial distribution of Mode-S EHS reports for London Heathrow and London Gatwick, received between 1200 to 1300 on 4 January 2015. London Gatwick is located 40 km south east of London Heathrow airport. At this time the air traffic flow was east to west, with aircraft arriving from the east and departing to the west. Each domain extends for a distance of 80 km east-west, 40 km north-south, height 3000 m from the surface, with the airport at the domain's centre. Points where the aircraft's roll angle is greater than $5°$, i.e. when turning, are removed since these data are considered unreliable. While the domains appear to be cuboid this is not the case. The sampled volume of space resembles an inverted truncated pyramid. Figures 10 and 11 we show the vertical temperature profile for the London Gatwick domain for two separate time periods. The method used to compute the $\overline{T}_{\mathrm{MACH}}$ observations is described in section 5.1.

In figure 10, as noted in section 5.1, the Herstmonceux (45 km south east of Gatwick) radiosonde temperature profile (black line) shows that temperature inversions are present. The UKV temperature profile forecasts a low-level temperature inversion between 150 m and 300 m. The $\overline{T}_{\mathrm{MACH}}$ observations suggest that the upper-level inversion is at 1600 m rather than around 2000 m shown by the radiosonde. Furthermore, the $\overline{T}_{\mathrm{MACH}}$ observations suggest that there is an isothermal region between 800 m and 1600 m, which is not shown by the UKV forecast or radiosonde. We note that there were no AMDAR reports for this period and location. The $\overline{T}_{\mathrm{MACH}}$ observations suggest that the rate of decay of the temperature inversion was much slower than that shown by the UKV forecast.

In figure 11, as noted in section 5.1, the Herstmonceux radiosonde temperature profile (black line) shows that temperature inversions are present. The UKV forecasts similar temperature inversions, although lower down when compared with the radiosonde. For this period and location there were five AMDAR reports, however, these do not show clearly the location of the temperature inversions. The $\overline{T}_{\mathrm{MACH}}$ observations show clearly the presence of the upper-level inversion but suggest it is lower down than forecast.

In both these cases, the $\overline{T}_{\mathrm{MACH}}$ observations at low levels may not be reliable because of the low number of Mode-S EHS reports used to make these report, as indicated by the width of the 95% confidence intervals, and the general increase in error at levels below 1000 m. Nonetheless, the $\overline{T}_{\mathrm{MACH}}$ observations may provide useful information when compared alongside other in situ temperature observations.
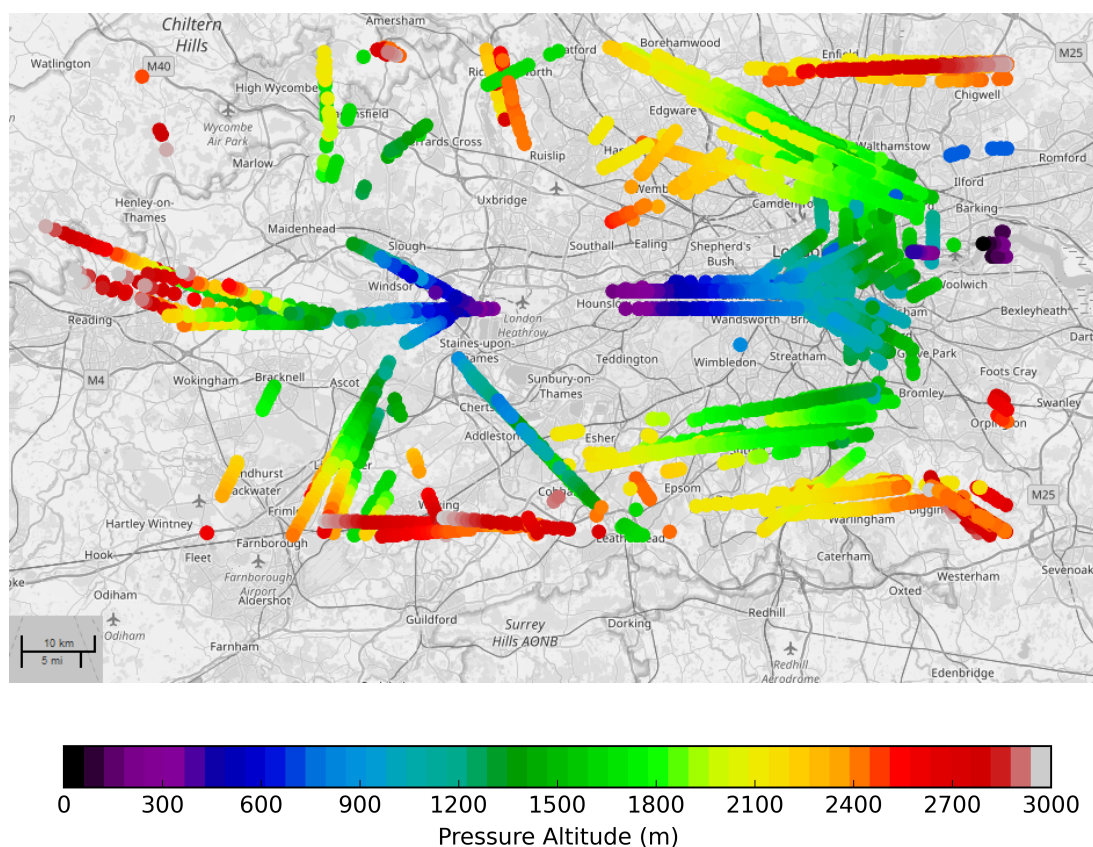
Figure 8: Spatial distribution of trajectories (circles, colour-coded by altitude) for ascending and descending aircraft within the London Heathrow domain, derived from Mode-S EHS reports received between 1200 to 1300 on 4 January 2015. (Cartography ©OpenStreetMap contributors, licensed as CC BY-SA https://www.openstreetmap.org/copyright, 2018)
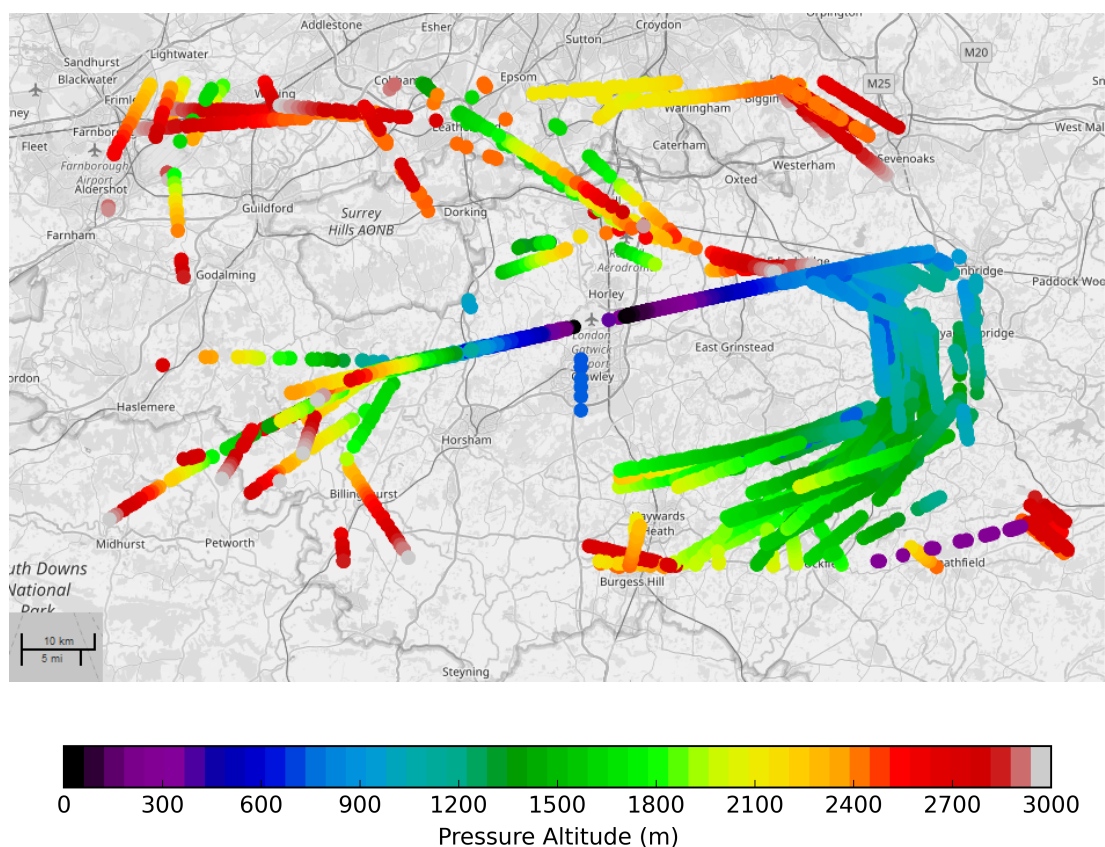
Figure 9: Spatial distribution of trajectories (circles, colour-coded by altitude) for ascending and descending aircraft within the London Gatwick domain, derived from Mode-S EHS reports received between 1200 to 1300 on 4 January 2015. (Cartography ©OpenStreetMap contributors, licensed as CC BY-SA https://www.openstreetmap.org/copyright, 2018)
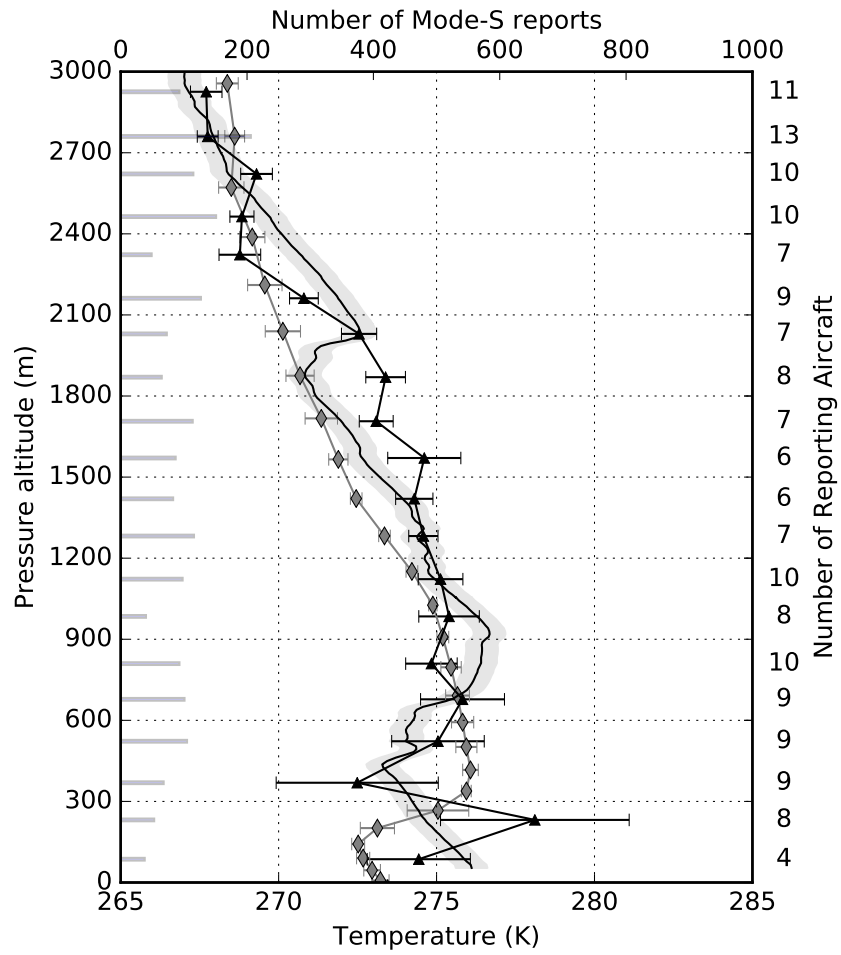
Figure 10: London Gatwick 2015-01-04, Mode-S EHS aggregated Mach Temperature vertical profiles (triangles), radiosonde (black) and mean UKV (narrow diamonds) temperature profiles. Symbols are as described in figure 2.
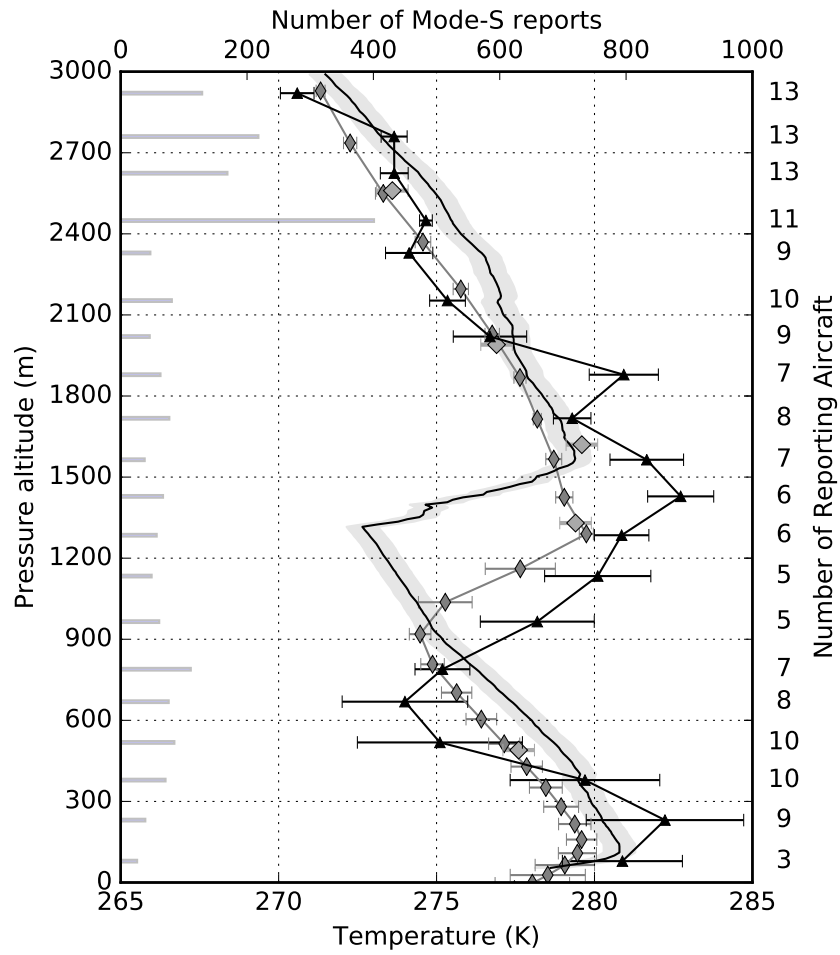
Figure 11: London Gatwick 2015-01-05, Mode-S EHS aggregated Mach Temperature vertical profiles (black triangles), radiosonde (black), available AMDAR reports (grey triangles) and mean UKV (narrow diamonds) temperature profiles. Symbols are as described in figure 2.

References

Ball, M., Barnhart, C., Nemhauser, G. and Odoni, A. (2007), Chapter 1 Air Transportation: Irregular Operations and Control, *in* 'Transportation', Elsevier, pp. 1–67.
  URL: *https://doi.org/10.1016/S0927-0507(06)14001-3*

Ballard, S. P., Li, Z., Simonin, D. and Caron, J.-F. (2015), 'Performance of 4D-Var NWP-based nowcasting of precipitation at the Met Office for summer 2012', *Quarterly Journal of the Royal Meteorological Society* **142**(694), 472–487.
  URL: *https://doi.org/10.1002/qj.2665*

Barnhart, C., Fearing, D., Odoni, A. and Vaze, V. (2012), 'Demand and capacity management in air transportation', *EURO Journal on Transportation and Logistics* **1**(1-2), 135–155.
  URL: *https://doi.org/10.1007/s13676-012-0006-9*

Boisvert, R. and Orlando, V. (1993), ADS-Mode S system overview, *in* 'Proceedings AIAA/IEEE Digital Avionics Systems Conference', IEEE.
  URL: *https://doi.org/10.1109/DASC.1993.283562*

Brown, R. (2004), *Smoothing, Forecasting and Prediction of Discrete Time Series (Reprint)*, Dover Phoenix Editions, Dover Publications.

Dance, S. L. (2004), 'Issues in high resolution limited area data assimilation for quantitative precipitation forecasting', *Physica D: Nonlinear Phenomena* **196**(1-2), 1–27.
  URL: *https://doi.org/10.1016/j.physd.2004.05.001*

de Haan, S. (2011), 'High-resolution wind and temperature observations from aircraft tracked by Mode-S air traffic control radar', *Journal of Geophysical Research* **116**(D10).
  URL: *https://doi.org/10.1029/2010jd015264*

de Haan, S. (2013), An improved correction method for high quality wind and temperature observations derived from Mode-S EHS. Technical report TR-338, Technical Report TR-338, Royal Netherlands Meteorological Institute, De Bilt, Netherlands.
  URL: *http://a.knmi2.nl/knmi-library/knmipubTR/TR338.pdf*

de Haan, S. and Stoffelen, A. (2012), 'Assimilation of High-Resolution Mode-S EHS Wind and Temperature Observations in a Regional NWP Model for Nowcasting Applications', *Weather and Forecasting* **27**(4), 918–937.
  URL: *https://dx.doi.org/10.1175/WAF-D-11-00088.1*

Drue, C., Frey, W., Hoff, A. and Hauf, T. (2008), 'Aircraft Type-Specific Errors In AMDAR

Weather Reports From Commercial Aircraft', *Quarterly Journal of the Royal Meteorological Society* **134**, 229–239.

Fowler, A., Bannister, R. and Eyre, J. (2011), 'A new floating model level scheme for the assimilation of boundary-layer top inversions: the univariate assimilation of temperature', *Quarterly Journal of the Royal Meteorological Society* **138**(664), 682–698.
URL: *https://doi.org/10.1002/qj.955*

Fowler, A. M. (2010), The assimilation of misplaced boundary layer features., PhD thesis, University of Reading.
URL: *http://centaur.reading.ac.uk/24800/*

Hoel, P. (1984), *Introduction to mathematical statistics*, Wiley series in probability and mathematical statistics, Wiley.

ICAO (1993), Manual of the ICAO Standard Atmosphere: Extended to 80 Kilometres (262 500 Feet) Third Edition, Technical Report Doc 7488-CD ISBN 92-9194-004-6, International Civil Aviation Organisation.

ICAO (2010), Annex 10 to the Convention on International Civil Aviation Aeronautical Telecommunications Volume IV Surveillance radar and Collision Avoidance Systems Ed 5, Technical report, International Civil Aviation Organisation.

Ingleby, B. and Edwards, D. (2014), 'Changes to radiosonde reports and their processing for numerical weather prediction', *Atmospheric Science Letters* **16**(1), 44–49.
URL: *https://doi.org/10.1002/asl2.518*

Jacobs, W., Nietosvaara, V., Bott, A., Bendix, J., Cermak, J., Michaelides, S. and Gultepe, I. (2008), *EUR 22978 COST Action 722 Earth System Science and Environmental Management Short range forecasting methods of fog, visibility and low clouds.*, Office for Official Publications of the European Communities.

Jacobs, W., Nietosvaara, V., Michaelides, S. C. and Gmoser, H. (2005), *EUR 21451 COST Action 722 Short-range Forecasting Methods of Fog, Visibility and Low Clouds - Phase I Report*, Office for Official Publications of the European Communities.

James, E. P. and Benjamin, S. G. (2017), 'Observation system experiments with the hourly updating rapid refresh model using gsi hybrid ensemble-variational data assimilation', *Monthly Weather Review* **145**(8), 2897–2918.
URL: *https://doi.org/10.1175/MWR-D-16-0398.1*

Kim, P. and Huh, L. (2011), *Kalman Filter for Beginners: With MATLAB Examples*, CreateS-pace Independent Publishing Platform.

Lange, H. and Janjic, T. (2016), 'Assimilation of Mode-S EHS Aircraft Observations in COSMO-KENDA', *Monthly Weather Review* **144**(5), 1697–1711.
URL: *https://doi.org/10.1175/MWR-D-15-0112.1*

Lean, H. W., Clark, P. A., Dixon, M., Roberts, N. M., Fitch, A., Forbes, R. and Halliwell, C. (2008), 'Characteristics of High-Resolution Versions of the Met Office Unified Model for Forecasting Convection over the United Kingdom', *Monthly Weather Review* **136**(9), 3408–3424.
URL: *https://doi.org/10.1175/2008MWR2332.1*

Mahashabde, A., Wolfe, P., Ashok, A., Dorbian, C., He, Q., Fan, A., Lukachko, S., Mozdzanowska, A., Wollersheim, C., Barrett, S. R., Locke, M. and Waitz, I. A. (2011), 'Assessing the environmental impacts of aircraft noise and emissions', *Progress in Aerospace Sciences* **47**(1), 15–52.
URL: *https://doi.org/10.1016/j.paerosci.2010.04.003*

Markovic, D., Hauf, T., Röhner, P. and Spehr, U. (2008), 'A statistical study of the weather impact on punctuality at Frankfurt Airport', *Meteorological Applications* **15**(2), 293–303.
URL: *https://doi.org/10.1002/met.74*

Mirza, A. K. (2017), On the Utilization of Aircraft Derived Observations for Operational Meteorology and Numerical Weather Prediction., PhD thesis, School of Mathematical, Physical and Computational Sciences, University of Reading.
URL: *http://centaur.reading.ac.uk/71981/*

Mirza, A. K., Ballard, S. P., Dance, S. L., Maisey, P., Rooney, G. G. and Stone, E. K. (2016), 'Comparison of aircraft-derived observations with in situ research aircraft measurements', *Quarterly Journal of the Royal Meteorological Society* **142**(701), 2949–2967.
URL: *https://doi.org/10.1002/qj.2864*

Oldham, K., Myland, J. and Spanier, J. (2010), *An Atlas of Functions: with Equator, the Atlas Function Calculator*, An Atlas of Functions, Springer New York.

Painting, C. (2003), *Aircraft Meteorological Data Relay (AMDAR) Reference Manual*, wmo no. 958 edn, World Meteorological Organisation, Secretariat of the World Meteorological Organization, Geneva, Switzerland.
URL: *http://www.wmo.int/pages/prog/www/GOS/ABO/AMDAR/AMDAR_System.html*

Rennie, S. J., Dance, S. L., Illingworth, A. J., Ballard, S. P. and Simonin, D. (2011), '3D-Var Assimilation of Insect-Derived Doppler Radar Radial Winds in Convective Cases Using a High-Resolution Model', *Monthly Weather Review* **139**(4), 1148–1163.
URL: *https://doi.org/10.1175/2010mwr3482.1*

Roach, W. T., Brown, R., Caughey, S. J., Garland, J. A. and Readings, C. J. (1976), 'The physics of radiation fog: I – a field study', *Quarterly Journal of the Royal Meteorological Society* **102**(432), 313–333.
URL: *https://doi.org/10.1002/qj.49710243204*

RTCA (2012), DO-339 Aircraft Derived Meteorological Data via Data Link for Wake Vortex, Air Traffic Management and Weather Applications - Operational Services and Environmental Definition (OSED)., Technical report, RTCA Washington.

Savitzky, A. and Golay, M. J. E. (1964), 'Smoothing and differentiation of data by simplified least squares procedures.', *Analytical Chemistry* **36**(8), 1627–1639.
URL: *https://doi.org/10.1021/ac60214a047*

Simonin, D., Ballard, S. P. and Li, Z. (2014), 'Doppler radar radial wind assimilation using an hourly cycling 3D Var with a 1.5 km resolution version of the Met Office Unified Model for nowcasting', *Quarterly Journal of the Royal Meteorological Society* **140**(684), 2298–2314.
URL: *https://doi.org/10.1002/qj.2298*

Stone, E. K. (2017), 'A comparison of mode-s enhanced surveillance observations with other in situ aircraft observations', *Quarterly Journal of the Royal Meteorological Society* .
URL: *https://rmets.onlinelibrary.wiley.com/doi/abs/10.1002/qj.3238*

Stone, E. K. and Kitchen, M. (2015), 'Introducing an approach for extracting temperature from aircraft gnss and pressure altitude reports in ADS-B messages', *Journal of Atmospheric and Oceanic Technology* **32**(4), 736–743.
URL: *https://doi.org/10.1175/JTECH-D-14-00192.1*

Stone, E. K. and Pearce, G. (2016), 'A Network of Mode-S Receivers for Routine Acquisition of Aircraft-Derived Meteorological Data', *Journal of Atmospheric and Oceanic Technology* **33**(4), 757–768.
URL: *https://doi.org/10.1175/jtech-d-15-0184.1*

Strajnar, B. (2012), 'Validation of mode-s meteorological routine air report aircraft observations', *Journal of Geophysical Research* **117**.
URL: *https://doi.org/10.1029/2012JD018315*

Strajnar, B., Aagar, N. and Berre, L. (2015), 'Impact of new aircraft observations Mode-S MRAR in a mesoscale NWP model', *Journal of Geophysical Research: Atmospheres* **120**(9), 3920–3938.
URL: *http://dx.doi.org/10.1002/2014JD022654*

Stull, R. (2000), *Meteorology for Scientists and Engineers*, Earth Science Series, Brooks Cole.

Sun, J., Xue, M., Wilson, J. W., Zawadzki, I., Ballard, S. P., Onvlee-Hooimeyer, J., Joe, P., Barker, D. M., Li, P.-W., Golding, B., Xu, M. and Pinto, J. (2014), 'Use of NWP for Nowcasting Convective Precipitation: Recent Progress and Challenges', *Bulletin of the American Meteorological Society* **95**(3), 409–426.
URL: *https://doi.org/10.1175/bams-d-11-00263.1*

Tang, Y., Lean, H. and Bornemann, J. (2013), 'The Benefits of the Met Office Variable Resolution NWP Model for Forecasting Convection', *Meteorological Applications* **20**(4), 417–426.
URL: *https://doi.org/10.1002/met.1300*

Wendisch, M. and Brenguier, J. (2013), *Airborne Measurements for Environmental Research: Methods and Instruments*, Wiley Series in Atmospheric Physics and Remote Sensing, Wiley.

World Meteorological Organisation (2014), 'Guide to Meteorological Instruments and Methods of Observation (WMO-No. 8) 2014 Edition', *World Meteorological Organisation, Geneva, Switzerland* .

Wright, D. J. (1986), 'Forecasting Data Published at Irregular Time Intervals Using an Extension of Holt's Method', *Management Science* **32**(4), 499–510.
URL: *https://doi.org/10.1287/mnsc.32.4.499*